REDUCED RISK OF NORTH AMERICAN COLD EXTREMES DUE TO CONTINUED ARCTIC SEA ICE LOSS

by James A. Screen, Clara Deser, and Lantao Sun

Contrary to recent claims, North American cold extremes are expected to become less frequent as a result of continuing Arctic sea ice loss.

In early January 2014, an Arctic air outbreak brought extreme cold to central and eastern North America. Record low minimum temperatures for the calendar date were set at many weather stations, including at Chicago, Illinois (O'Hare Airport, –26.7°C/–16°F, 6 January); New York, New York (Central Park, –15.6°C/4°F, 7 January); Washington, D.C. (Dulles Airport, –17.2°C/1°F, 7 January); and as far south as Atlanta, Georgia (–14.4°C/6°F, 7 January)

AFFILIATIONS: Screen—College of Engineering, Mathematics and Physical Sciences, University of Exeter, Exeter, United Kingdom; Deser and Sun—Climate and Global Dynamics, National Center for Atmospheric Research,* Boulder, Colorado

*The National Center for Atmospheric Research is sponsored by the National Science Foundation.

CORRESPONDING AUTHOR: James A. Screen, College of Engineering, Mathematics and Physical Sciences, University of Exeter, Laver Building, 6th FL., North Park Road, Exeter EX4 4QF, United Kingdom
E-mail: j.screen@exeter.ac.uk

The abstract for this article can be found in this issue, following the table of contents.

In final form 11 November 2014

and Austin, Texas (Bergstrom Airport, –11.1°C/12°F, 7 January).[1] Daily maximum snowfall records were also broken at several stations, including Buffalo, New York (7.6″, 8 January), and St. Louis, Missouri (10.8″, 5 January).

The cold temperatures and heavy snowfall caused widespread disruption to transport and power supply, closure of work places and public services, and damage to agricultural crops—all with significant economic implications. Unsurprisingly, given the disruption, the national and global media extensively reported the cold snap, including debate on whether human-induced climate change was partly responsible. Related to this, one particular hypothesis garnered considerable attention: the suggestion that rapid Arctic warming and associated sea ice loss may be increasing the risk of cold extremes.

The media were not alone in making this link. In the midst of the frigid conditions, the White House released a public information video claiming that, paradoxically, cold extremes will become more likely as a result of global warming. President Obama's Science Advisor, Dr. John Holdren, stated that "the

---

[1] Data from the National Weather Service (www.nws.noaa.gov/climate).

kind of extreme cold being experienced by much of the United States as we speak is a pattern that we can expect to see with increasing frequency as global warming continues."

The cited explanation was that Arctic sea ice loss specifically, or Arctic amplification (the greater warming of the Arctic than lower latitudes) more generally, is increasing the likelihood of the type of weather patterns that lead to cold extremes. The scientific basis for this statement is derived from a number of recent observational and modeling studies (Honda et al. 2009; Petoukhov and Semenov 2010; Francis and Vavrus 2012; Inoue et al. 2012; Liu et al. 2012; Yang and Christensen 2012; Tang et al. 2013; Cohen et al. 2014; Vihma 2014; Walsh 2014).

However, key aspects of some of these aforementioned studies have been questioned (Barnes 2013; Screen and Simmonds 2013; Barnes et al. 2014; Gerber et al. 2014; Woollings et al. 2014) and counterarguments put forward (Hassanzadeh et al. 2014; Fischer and Knutti 2014; Screen 2014; Wallace et al. 2014). Furthermore, these studies have largely focused on relationships in the present-day climate. Only a few studies have considered the global impacts of future sea ice loss (e.g., Deser et al. 2010; Peings and Magnusdottir 2014; Deser et al. 2015) and these have

focused on seasonal-mean changes. Future changes in cold extremes in response to projected Arctic sea ice loss require further study. Here we specifically focus on North America, prompted by the events of winter 2013/14 and the extensive media coverage it received.

HOW UNUSUAL WAS WINTER 2013/14?

We start with a brief overview of the winter of 2013/14, based on gridded temperature data from the National Centers for Environmental Prediction–National Center for Atmospheric Research (NCEP–NCAR) reanalysis (Kalnay et al. 1996). The period December 2013 through February 2014 was, on average, anomalously cold over most of North America east of the Rocky Mountains (Fig. 1a), while the Southwest United States and northeast Canada were anomalously warm. The winter of 2013/14 was punctuated by several cold air outbreaks, the most severe of which occurred around 7 January 2014. Compared to the daily average for this date in period 1980–99, the largest anomalies on 7 January 2014 were experienced in the eastern United States, with −20°C anomalies stretching from Ohio to as far south as Florida (Fig. 1b). Averaged over central to eastern North America (CENA; 26°–58°N, 70°–100°W; black box in Fig. 1b), daily mean temperatures were well below average for
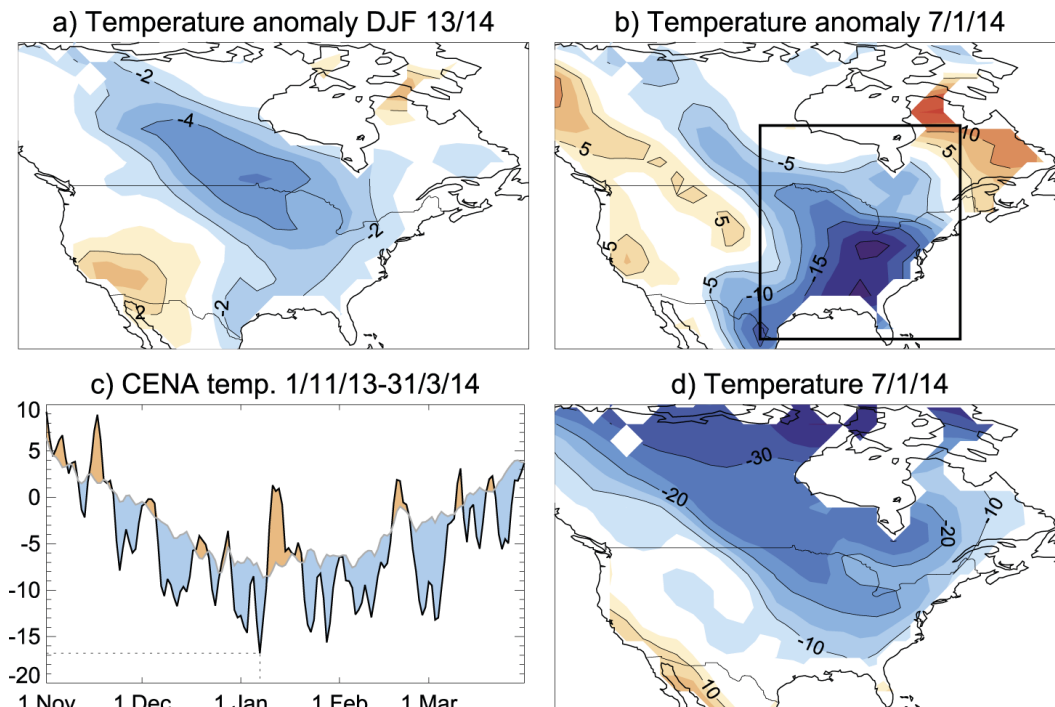

FIG. 1. North American temperature anomalies for (a) the winter of 2013/14 and (b) 7 Jan 2014. Anomalies are relative to the period 1980–99. (c) Daily mean temperature averaged over CENA [black box in (b)] for 1 Nov 2013–31 Mar 2014 (black curve) and the daily 1980–99 climatology (gray line). Blue (orange) shading shows days colder (warmer) than the average for that day. (d) North American temperatures for 7 Jan 2014.
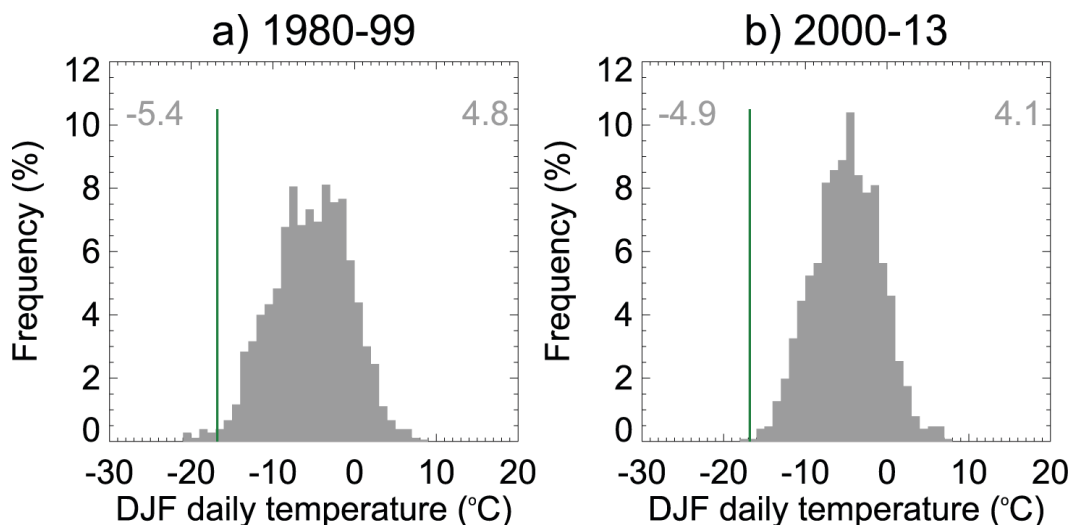
a) 1980-99

-5.4 ... 4.8

b) 2000-13

-4.9 ... 4.1

Fɪɢ. 2. (a) Histogram of daily winter temperatures averaged over CENA during the period 1980–99. (b) As in (a), but based on the period 2000–13. Green lines are drawn at −16.8°C and correspond to the temperature on 7 Jan 2014. Numbers in the top left and top right of each panel are the mean temperature (°C) and standard deviation (°C), respectively.

large portions of the winter (Fig. 1c). The coldest daily mean temperature over CENA during the winter of 2013/14 occurred on 7 January, recording −16.8°C. On this day, temperatures averaged below −20°C over central Canada and west of the Great Lakes and below −10°C over most of the United States east of the Rockies (Fig. 1d).

Next, we consider how "extreme" the cold conditions were over CENA on 7 January 2014. Figure 2a shows the probability distribution function (PDF) of daily mean temperatures, averaged over CENA, during the winter months of the late twentieth century (1980–99). The vertical green line is drawn at −16.8°C, corresponding to the mean temperature on 7 January 2014. The 7 January event falls in the tail of the distribution, but it is not unprecedented in the recent past. The coldest day over this period occurred on 19 January 1994 (−20.3°C). During 1980–99, 20 days had a daily mean CENA temperature as cold or colder than −16.8°C, spread across six winters (Table 1). Such events have often occurred in clusters, with multiple days this cold in several years. Based on the 1980–99 PDF (Fig. 2a), the 7 January 2014 event has a probability of 1.1%, which equates to an average return period of one year (since there are 90 winter days per year). Viewed in this light, the recent event does not seem to be a rare occurrence.

At first glance it may seem odd that so many long-term station records were broken on 7 January 2014, if an event of such severity is not uncommon. However, the records referred to in the opening paragraph, and comparable records widely quoted in the media

reporting of this event, refer to the fact that the temperature on 7 January 2014 was colder than those on the same date in previous years, but it was not necessarily colder than on all dates in previous years. Cold extremes occur throughout the winter and not always on the same date. For example, days equally cold or colder than −16.8°C over CENA since 1980 have occurred on dates from mid-December to early February (Table 1) but only once on 7 January—and that was in 2014. The probability of a cold extreme occurring on a particular date is therefore much smaller than the probability of it occurring on any date. Hence, the breaking of records for a particular date is not necessarily a good measure of how extreme an event is.

A somewhat different perspective on the extremity of the 7 January event arises if a more recent reference period is considered. Figure 2b shows an analogous PDF based on daily winter CENA temperature during the period 2000–13. Arctic sea ice loss has accelerated in this period (Stroeve et al. 2012), so if there were a detectable influence of sea ice loss on cold extremes, we would expect to see it over this time period. Between 2000 and 2013, only one day (16 January 2009) was colder than −16.8°C, giving a probability of 0.08% (one day in 14 years). Thus, the 7 January 2014 event could be perceived as extreme compared to temperature minima in the early twenty-first century, which may help explain the media and public perception of this event being extreme. However, clearly this event was not uncommon in a longer-term context. Only a decade or two earlier, events of comparable magnitude occurred

TABLE 1. Days equally as cold or colder than 7 Jan 2014 over CENA since 1980, based on the NCEP–NCAR reanalysis.

Date	CENA *T* (°C)	Date	CENA *T* (°C)	Date	CENA *T* (°C)
25 Dec 1980	−16.8	25 Dec 1983	−20.2	18 Jan 1994	−17.5
10 Jan 1982	−18.2	20 Jan 1984	−17.9	19 Jan 1994	−20.3
11 Jan 1982	−18.6	21 Jan 1984	−17.4	1 Feb 1996	−18.4
17 Jan 1982	−20.1	22 Dec 1989	−20.2	2 Feb 1996	−18.2
19 Dec 1983	−17.5	23 Dec 1989	−19.6	3 Feb 1996	−20.2
20 Dec 1983	−17.2	15 Jan 1994	−18.2	4 Feb 1996	−19.8
24 Dec 1983	−18.1	16 Jan 1994	−18.4	16 Jan 2009	−17.2

relatively frequently. This simple comparison suggests that cold extremes are becoming less frequent, not more frequent, consistent with previous studies (Alexander et al. 2006; Donat et al. 2013) and the anticipated response to global warming (Kharin et al. 2007, 2013). However, such interpretation must be treated with caution, as the time periods considered are very short with few extremes (by definition) upon which to calculate robust statistics.

MODELS AND SIMULATIONS. We now turn our attention to quantifying future changes in CENA cold extremes, with particular focus on the projected changes driven by continued Arctic sea ice loss. To do this, we analyze large ensembles of coupled model simulations that have been forced by greenhouse gas (GHG) increases and that produce reductions in Arctic sea ice (Stroeve et al. 2012), among other impacts, and ensembles of atmospheric model simulations forced by solely the GHG-induced Arctic sea ice loss with all other forcing factors held constant.

To estimate the response to projected increases in GHG, we utilize coupled climate model simulations from the fifth phase of the Coupled Model Intercomparison Project (CMIP5; Taylor et al. 2012). We chose to use the representative concentration pathway 8.5 (RCP8.5), which is a high-end ("business as usual") scenario with a rapid rise in GHG concentrations through the twenty-first century, for two reasons: first, to maximize the signal-to-noise ratio, and second, because observed Arctic sea ice reductions track those simulated under RCP8.5 more closely than those under any of the lower-end scenarios (Stroeve et al. 2012). We sample the projections at two time periods, 2030–49 and 2080–99, representative of the mid-twenty-first century (C21) and late C21, respectively. The projections are compared to the baseline period 1980–99, representative of the late twentieth

century (C20). Data for this period come from the CMIP5 historical simulations of the models. The historical simulations have all been forced with observed concentrations of GHG, aerosols, ozone, and natural forcings (solar, volcanic eruptions) from 1850 to 2005. We analyzed one ensemble member from each of the 34 models that had all necessary data available for the historical and RCP8.5 experiments.

To isolate the influence of sea ice, we performed atmospheric model simulations with prescribed sea ice concentration, sea ice thickness, and sea surface temperature (SST). For this we used the atmospheric components of the Hadley Centre Global Environmental Model, version 2 (HadGEM2; Collins et al. 2011), and the Community Climate System Model, version 4 (CCSM4; Gent et al. 2011)—namely, the Hadley Centre Global Atmospheric Model, version 2 (HadGAM2), and the Community Atmosphere Model, version 4 (CAM4), respectively. The version of HadGAM2 used here has a horizontal resolution of 1.875° longitude × 1.25° latitude and 38 vertical levels. CAM4 has a horizontal resolution of 1.25° longitude × 0.9° latitude and 26 vertical levels. We performed three experiments using both models, each experiment having repeating seasonal cycles of sea ice conditions representative of a different time period—the late C20, the mid-C21, and the late C21 (as defined above). These sea ice conditions were taken from the CMIP5 integrations of HadGEM2-ES and CCSM4 (i.e., sea ice from HadGEM2-ES was prescribed in HadGAM2 and sea ice from CCSM4 was prescribed in CAM4), averaged across the 20 years of the chosen period and all available ensemble members. Specifically, we used five HadGEM2-ES historical runs, four HadGEM2-ES RCP8.5 runs, six CCSM4 historical runs, and six CCSM4 RCP8.5 runs. In the HadGAM2 experiments, sea ice thickness was derived empirically from the sea ice concentrations. In the CAM4 simulations, the prescribed sea ice thicknesses were

based on climatologies from the CCSM4 simulations for each period (the late C20, the mid-C21, and the late-C21; i.e., in the same manner as the sea ice concentrations). The treatment of SST was as follows. In the C20 experiment, SSTs were held to the climatology of the late C20, using the ensemble-mean SST from the HadGEM2-ES and CCSM4 historical simulations. In the mid- and late C21 experiments, the SST was also held to the climatology of the late C20, except at grid boxes where sea ice was lost. At these locations, the climatological SST of the mid-C21 or late C21 was used, taken from the HadGEM2-ES and CCSM4 RCP8.5 ensemble means. This procedure accounts for the local SST warming associated with reduced sea ice cover, but it excludes remote SST changes that are not directly tied to the ice loss (see Screen et al. 2013; Deser et al. 2015). The three experiments were each run for 260 years. In this modeling framework, each model year can be considered an independent ensemble member starting from a different atmospheric initial condition. By running very large ensembles, we aim to fully capture the large intrinsic atmospheric variability. The details of each model experiment are summarized in Tables 2 and 3.

CONTINUED ARCTIC SEA ICE LOSS.
Ensemble-mean winter sea ice concentrations in HadGEM2-ES during the late C20 and the mid- and late C21 are shown in Figs. 3a–c, respectively. The projected loss of sea ice in the mid-C21, relative to the late C20, is fairly small (–1.5 million km²). The largest local changes in sea ice cover are found in the Barents Sea (cf. Figs. 3a,b). By late C21, however, HadGEM2-ES simulates almost ice-free conditions in winter (Fig. 3c). Ice cover is maintained predominantly in coastal regions and embayments. Analogous plots for CCSM4 are shown in Figs. 3d–f. CCSM4 also simulates a modest change in winter sea ice cover between the late C20 and the mid-C21 (–1.3 million km²). The largest changes in sea ice cover in CCSM4, in the late C21 relative to the late C20, are found in the Bering, Beaufort, and Chukchi Seas (Fig. 3f). In the late C21, CCSM4 simulates considerably more winter ice (8.6 million km²) than HadGEM2-ES (3.5 million km²). The change in winter sea ice area between the late C20 and the late C21 is –10.3 and –4.8 million km², as simulated by HadGEM2-ES and CCSM4, respectively.

Figure 3g shows the winter sea ice area changes in these two models overlaid on the projected changes

Model(s)	Forcing	Time period analyzed	Ensemble members	Years of simulation
CMIP5	Historical	1980–99	34*	680
	RCP8.5	2030–49	34*	680
	RCP8.5	2080–99	34*	680
HadGEM2-ES	Historical (A)	1980–99	5	100
	RCP8.5 (B)	2030–49	4	80
	RCP8.5 (C)	2080–99	4	80
CCSM4	Historical (D)	1980–99	3	60
	RCP8.5 (E)	2030–49	6	120
	RCP8.5 (F)	2080–99	6	120
HadGAM2	Mean sea ice from A, SST from A	Annually repeating	260	260
	Mean sea ice from B, SST from A	Annually repeating	260	260
	Mean sea ice from C, SST from A	Annually repeating	260	260
CAM4	Mean sea ice from D, SST from D	Annually repeating	260	260
	Mean sea ice from E, SST from D	Annually repeating	260	260
	Mean sea ice from F, SST from D	Annually repeating	260	260

TABLE 2. Details of the model simulations analyzed. Asterisk means one ensemble member per model. The 34 CMIP5 models analyzed are listed in Table 3.

TABLE 3. The names of the 34 CMIP5 models.	
Acronym	**Expansion**
ACCESS1.0	Australian Community Climate and Earth-System Simulator, version 1.0
ACCESS1.3	Australian Community Climate and Earth-System Simulator, version 1.3
BCC_CSM1.1	Beijing Climate Center, Climate System Model, version 1.1
BCC_CSM1.1(m)	Beijing Climate Center, Climate System Model, version 1.1 (moderate resolution)
BNU-ESM	Beijing Normal University–Earth System Model
CanESM2	Second Generation Canadian Earth System Model
CCSM4	Community Climate System Model, version 4
CESM1-BGC	Community Earth System Model, version 1 (biogeochemistry)
CESM1(CAM5)	Community Earth System Model, version 1 (Community Atmosphere Model, version 5)
CMCC-CESM	Centro Euro-Mediterraneo per I Cambiamenti Climatici Carbon Cycle Earth System Model
CMCC-CM	Centro Euro-Mediterraneo per I Cambiamenti Climatici Climate Model
CMCC-CMS	Centro Euro-Mediterraneo per I Cambiamenti Climatici Stratosphere-Resolving Climate Model
CNRM-CM5	Centre National de Recherches Météorologiques Coupled Global Climate Model, version 5
CSIRO Mk3.6.0	Commonwealth Scientific and Industrial Research Organisation Mark 3.6.0
EC-EARTH	European Consortium Earth System Model
GFDL CM3	Geophysical Fluid Dynamics Laboratory Climate Model, version 3
GFDL-ESM2G	Geophysical Fluid Dynamics Laboratory Earth System Model with the Generalized Ocean Layer Dynamics (GOLD) component
GFDL-ESM2M	Geophysical Fluid Dynamics Laboratory Earth System Model with the Modular Ocean Model (MOM), version 4 component
GISS-E2-H	Goddard Institute for Space Studies Model E2, coupled with the Hybrid Coordinate Ocean Model (HYCOM)
GISS-E2-R	Goddard Institute for Space Studies Model E2, coupled with the Russell ocean model
HadGEM2-CC	Hadley Centre Global Environment Model, version 2–Carbon Cycle
HadGEM2-ES	Hadley Centre Global Environment Model, version 2–Earth System
INM-CM4.0	Institute of Numerical Mathematics Coupled Model, version 4.0
IPSL-CM5A-LR	L'Institut Pierre-Simon Laplace Coupled Model, version 5A, low resolution
IPSL-CM5A-MR	L'Institut Pierre-Simon Laplace Coupled Model, version 5A, medium resolution
IPSL-CM5B-LR	L'Institut Pierre-Simon Laplace Coupled Model, version 5B, low resolution
MIROC-ESM	Model for Interdisciplinary Research on Climate, Earth System Model
MIROC-ESM-CHEM	Model for Interdisciplinary Research on Climate, Earth System Model, Chemistry Coupled
MIROC5	Model for Interdisciplinary Research on Climate, version 5
MPI-ESM-LR	Max Planck Institute Earth System Model, low resolution
MPI-ESM-MR	Max Planck Institute Earth System Model, medium resolution
MRI-CGCM3	Meteorological Research Institute Coupled Atmosphere–Ocean General Circulation Model, version 3
MRI-ESM1	Meteorological Research Institute Earth System Model, version 1
NorESM1-M	Norwegian Earth System Model, version 1 (intermediate resolution)

in all the CMIP5 models. In the late C20 and the mid-C21, both models have a winter sea ice cover close to the CMIP5 ensemble mean. In the late C21, the two models diverge from the CMIP5 mean. HadGEM2-ES simulates considerably less winter ice than the CMIP5 mean, whereas CCSM4 simulates more winter ice than the CMIP5 mean. Both models, however, lie within the 10%–90% range of the CMIP5 model spread. Thus, we consider the simulations by these two models to capture some of the uncertainty in future sea ice cover, but neither of the models are obvious outliers. In terms of winter sea ice volume, CCSM4 lies near to the CMIP5 mean in all three time periods (Fig. 3h). HadGEM2-ES has a winter sea ice volume close to

the CMIP5 mean in the late C20 and the late C21, but it has a larger volume in the mid-C21 (primarily due to thicker ice). We note that the sea ice thicknesses used to calculate these values are those derived empirically from the sea ice concentration (and prescribed to HadGAM2; see above) and not those simulated in the HadGEM2-ES RCP8.5 experiment.

WARMER AND LESS VARIABLE. Figure 4a shows PDFs of winter daily CENA temperature from 34 CMIP5 models. The three histograms show distributions based on the late C20 (gray bars), the mid-C21 (blue), and the late C21 (red). Each histogram is based upon 61,200 daily values (34 models × 20 years × 90 days). As a group, the CMIP5 models project a shift toward the right and a narrowing of the PDF, the former implying mean warming and the latter less variability. The mean warming measures 2.6°C by the mid-C21 and 6.5°C by the late C21, both relative to the late C20. The standard deviation decreas-

FIG. 3. Ensemble-mean winter sea ice concentrations from **HadGEM2-ES** during the period (a) 1980–99, (b) 2030–49, and (c) 2080–99. (d)–(f) As in (a)–(c), but for **CCSM4**. (g) Evolution of winter sea ice area in the CMIP5 historical and RCP8.5 experiments, 1980–2099. Blue curve denotes the multimodel mean, dense hatching denotes the 10%–90% range of the model spread, and light hatching denotes the full model spread. Black and green lines show the values prescribed in the sea ice–forced **HadGAM2** and **CAM4** simulations, respectively. (h) As in (g), but for sea ice volume.

es by –0.3°C by the mid-C21 and by –0.7°C by the late C21, again relative to the late C20. All these changes are statistically significant (95% confidence).

Figures 4b,c show analogous PDFs from simulations of the HadGEM2-ES and CCSM4 models, respectively. We present the simulations from Had-GEM2-ES and CCSM4 here to enable direct comparisons with the sea ice–forced runs that were conducted with the atmospheric components of these coupled models. Both models show broadly the same response as the CMIP5 ensemble—namely, mean warming and a decrease in variability. The HadGEM2-ES simulations show warming of 3.5° and 8.7°C in the mid- and the late C21, respectively, and variability
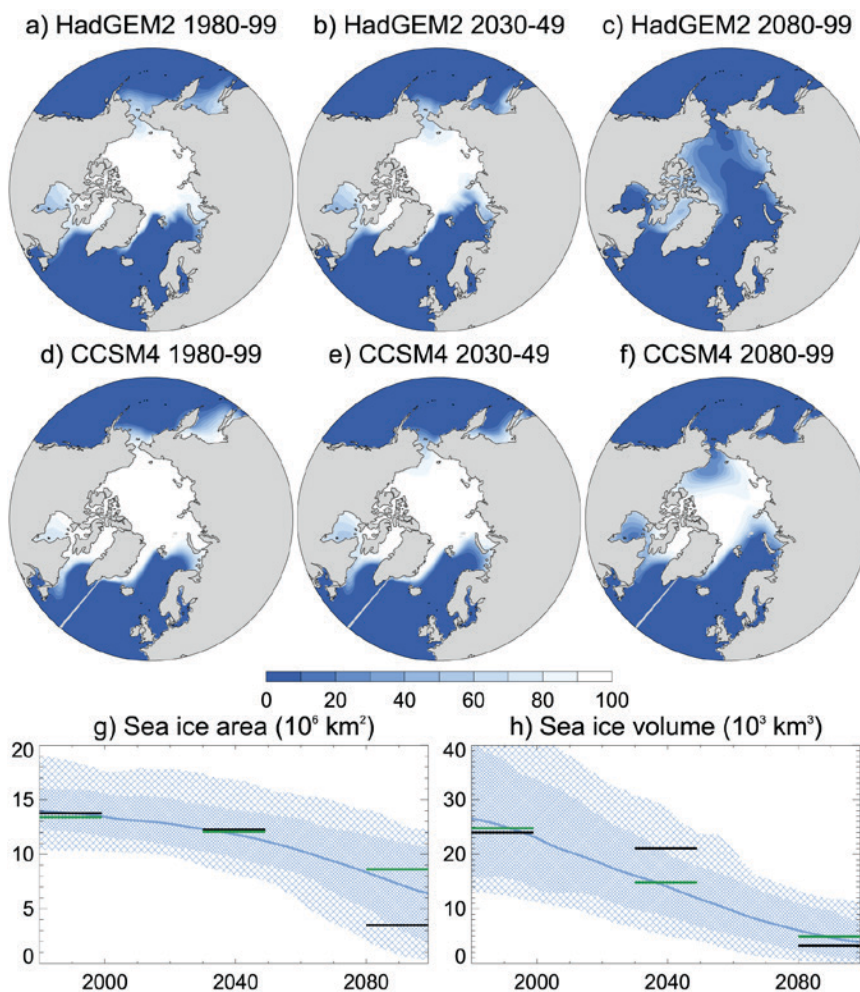
declines of –0.3° and –1.1°C in the mid- and late C21, respectively. The CCSM4 simulations show a mean warming of 2.6°C by the mid-C21 and 5.7°C by the late C21 and a standard deviation decrease of –0.24°C by the mid-C21 and –0.58°C by the late C21. Again, all quoted changes are statistically significant (95% confidence).

The results from the sea ice–forced experiments are shown in Figs. 4d,e for HadGAM2 and CAM4, respectively. As under GHG forcing, the sea ice–forced simulations show mean warming and a decrease in variability, but to a lesser degree than in the GHG-forced experiments. The sea ice–forced changes in mean temperature and standard deviation are relatively
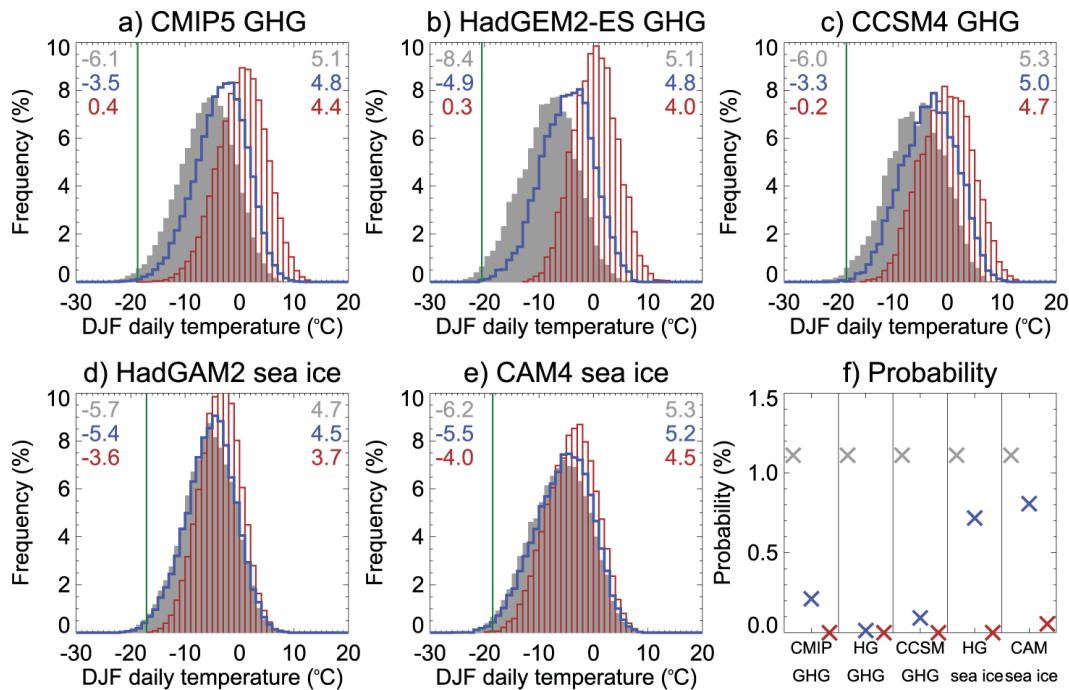
Fig. 4. (a) **Histograms of simulated daily winter temperature averaged over CENA taken from 34 coupled climate models for the periods 1980–99 (gray bars), 2030–49 (blue), and 2088–99 (red). Numbers in the top left and top right of each panel are the mean temperature (°C) and standard deviation (°C), respectively. Vertical green line denotes the value of the model's 1.1 percentile, the simulated analog of the 7 Jan 2014 event in observations.** (b)–(e) **As in (a), but for coupled simulations with (b) HadGEM2-ES and (c) CCSM4 and for sea ice–forced simulations with (d) HadGAM2 and (e) CAM4.** (f) **Probability of daily temperature as cold or colder than the 1.1 percentile in the period 1980–99 in each model ensemble and period.**

small between the late C20 and the mid-C21, but they emerge more clearly by the late C21, consistent with the magnitude of the sea ice loss (recall Fig. 3g). HadGAM2 simulates warming of 0.3°C by the mid-C21 and 2.0°C by the late C21, and CAM4 exhibits warming of 0.7° and 2.2°C, respectively (all statistically significant). These CENA temperature changes can be divided by the changes in winter sea ice area to yield sensitivity terms. In HadGAM2 this sensitivity is 0.2°C (million km)$^{-2}$ (multiplied by –1 to yield a value for sea ice area loss) between the late C20 and the mid-C21 and the same value between the mid- and late C21. In CAM4 the corresponding values are 0.5 and 0.4°C (million km)$^{-2}$. Thus, in both models there is an approximately linear relationship between winter sea ice area loss and CENA warming; however, CAM4 has a higher sensitivity than HadGAM2. Both models simulate a statistically significant decrease in the standard deviation of CENA temperature by the late C21 in response to sea ice loss, –1.0°C in HadGAM2 and –0.8°C in CAM4, which represents a 27% and 18% decrease relative to the late C20, respectively. Although much smaller in magnitude, a statistically significant decrease in variability in response to sea ice loss is

evident by the mid-C21 in both models. None of the C21 sea ice–forced experiments show evidence of cooling or increased variability relative to the C20: in other words, there is no evidence for increased cold extremes.

So, why does Arctic sea ice loss make CENA temperature warmer and less variable? Arctic sea ice loss drives local warming via changes in the surface heat fluxes (Deser et al. 2010; Screen and Simmonds 2010a,b; Screen et al. 2013). This warming signal is spread to lower latitudes primarily due to temperature advection by transient eddies (Deser et al. 2010). Temperature advection can also help explain the variability decrease. Cold winter days in the midlatitudes tend to coincide with northerly wind (from the Arctic) and warm winter days with southerly wind (from the subtropics). Arctic warming, induced by sea ice loss, leads to warmer northerly wind but little change in temperature of southerly wind (Screen 2014). As a result, cold days warm faster than warm days, leading to a decrease in daily temperature variability (Screen 2014). Figure 4 clearly shows that the cold (left hand) tail of the CENA temperature PDF warms more (i.e., shifts farther to the right) than does the warm (right hand) tail, supporting this simple mechanism.

Contrasting the GHG-forced and sea ice–forced simulations, sea ice loss in HadGAM2 explains 9% of the mean warming and 52% of the decreased standard deviation seen in HadGEM2-ES between the late C20 and the mid-C21, and sea ice loss in CAM4 accounts for 25% of the mean warming and 58% of the decreased standard deviation seen in CCSM4 in the CENA region (Table 4). By the late C21, sea ice loss accounts for 24% of the mean warming and 87% of the decreased standard deviation in HadGEM2-ES and 38% of the mean warming and 141% of the decreased standard deviation in CCSM4. The latter percentage, being larger than 100%, implies that other processes (not directly related to Arctic sea ice loss) in the GHG-forced experiment are responsible for an increase in variability that partially offsets the sea ice–driven variability decrease. Evidently Arctic sea ice loss is the key driver of the projected decrease in variability by the late C21, supporting similar conclusions for the midlatitudes as a whole (Screen 2014).

REDUCED RISK OF COLD EXTREMES. For each experiment, we identified a threshold CENA temperature that occurs with 1.1% (one day per year) frequency during the late C20. This represents the model analog to 7 January 2014. We note that because the models are generally biased cold relative to the reanalysis, the chosen threshold temperatures are lower than −16.8°C (−18.7°, −20.5°, −18.6°, −17.1°, and −18.5°C for the CMIP5, HadGEM2-ES, CCSM4, HadGAM2, and CAM4 simulations, respectively). Figure 4f shows how the probability of CENA temperature equal to or below this threshold changes in the future in response to increased GHG and to Arctic sea ice loss. In the CMIP5 models, the probability reduces to 0.21% (one day in five years) by the mid-C21. By the late C21, the CENA temperature never equals or falls below the threshold. In the HadGEM2-ES coupled simulations, the probability reduces to 0.014% (one day in 80 years) by the mid-C21 and, again, reduces to zero by the late

C21. The probability reduces to 0.093% (one day in 12 years) and zero in the CCSM4 simulations by the mid-C21 and the late C21, respectively. Thus, by the mid-C21, increased GHG reduce the odds of an event as severe as 7 January 2014 by a factor of 5 based on the CMIP5 models as a group, a factor of 80 based on HadGEM2-ES, and a factor of 12 based on CCSM4.

In response to projected sea ice loss, the probability of CENA temperature below the threshold temperature reduces to 0.7% (one day in 1.6 years) in HadGAM2 and to 0.8% (one day in 1.4 years) in CAM4 by the mid-C21. Thus, projected Arctic sea ice loss alone reduces the odds of such an event by one-quarter to one-third in the mid-C21 compared to late C20. By late C21, the probability falls to zero in HadGAM2 and 0.06% (one day in 19 years) in CAM4.

The sea ice–forced simulations presented here were not coupled to an ocean model and, thus, ocean feedbacks are not represented. Deser et al. (2015) examined the climate response to projected Arctic sea ice in coupled and uncoupled versions of CCSM4. These authors show that the coupled response to Arctic sea ice loss resembles a weaker version of the full response to GHG in CCSM4. Since North American warming and decreased temperature variance are robust characteristics of the full coupled response to GHG, we speculate that ocean feedbacks may further reduce the risk of cold extremes or, at least, are unlikely to increase the risk.

HEMISPHERIC PERSPECTIVE. A wider geographical perspective on the simulated response to sea ice loss is provided in Fig. 5, which shows maps of mean temperature and standard deviation change between the late C20 and the mid-C21. Both models show warming over the high-latitude continents (Figs. 5a,c), accompanied by a decrease in standard deviation (Figs. 5b,d). Both the warming and variability decrease are more widespread in CAM4 than in HadGAM2. By the late C21, both models depict larger warming over the

TABLE 4. Changes in winter daily mean CENA temperature and variance simulated in response to GHG increases and Arctic sea ice decreases. Numbers in parentheses denote the percentage of simulated change under GHG forcing that can be explained solely by projected Arctic sea ice loss. All changes are statistically significant at the 95% confidence level.

Model	Period	Temperature change relative to 1980–99 (°C)		Std dev change relative to 1980–99 (°C)	
		GHG	Sea ice	GHG	Sea ice
HadGEM2-ES/ HadGAM2	2030–49	3.49	0.32 (9%)	−0.31	−0.16 (52%)
	2080–99	8.67	2.08 (24%)	−1.11	−0.97 (87%)
CCSM4/CAM4	2030–49	2.62	0.65 (25%)	−0.24	−0.14 (58%)
	2080–99	5.74	2.17 (38%)	−0.58	−0.82 (141%)

a) HadGAM2 mean

b) HadGAM2 standard deviation

c) CAM4 mean

d) CAM4 standard deviation

Mean temperature difference (°C)
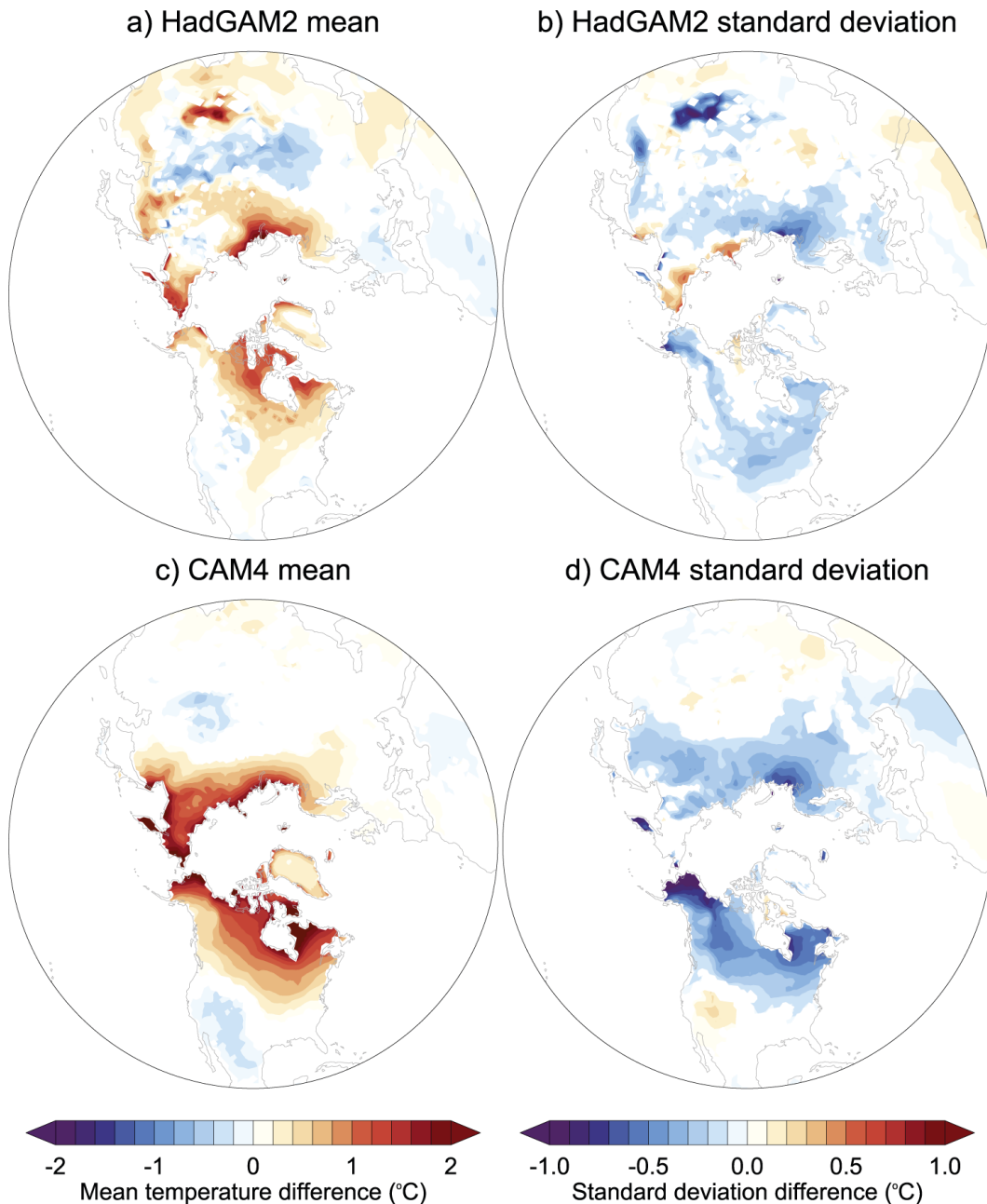
Standard deviation difference (°C)

FIG. 5. **Differences in (a) mean winter near-surface air temperature and (b) standard deviation of daily winter near-surface air temperature between the periods 2030–49 and 1980–99 in the HadGAM2 sea ice–forced experiments. (c),(d) As in (a),(b), but for the CAM4 sea ice–forced experiments. Colored shading is shown only at grid points where the difference is statistically significant at the 95% confidence level.**

high-latitude continents and an extension of the warming signal into parts of the midlatitudes (Fig. 6). In particular, warming is simulated over much of the eastern United States. Also by the late C21, there are larger-magnitude and more widespread simulated reductions in standard deviation, with significant decreases over most of North America, Russia, and northern Europe by the late C21. In contrast, both models depict weak cooling and patches of increased standard deviation over eastern Asia (China, Mongolia). This cooling is related to a simulated strengthening of the Siberian high (not shown), consistent with the model results of Mori et al. (2014). It is noteworthy that the two models depict a robust spatial pattern of mean temperature and variability change in response to Arctic sea ice loss.

These changes in mean temperature and variability due to Arctic sea ice loss would be expected to translate into altered frequencies of cold extremes. To show this

a) HadGAM2 mean

b) HadGAM2 standard deviation

c) CAM4 mean

d) CAM4 standard deviation

Mean temperature difference (°C)

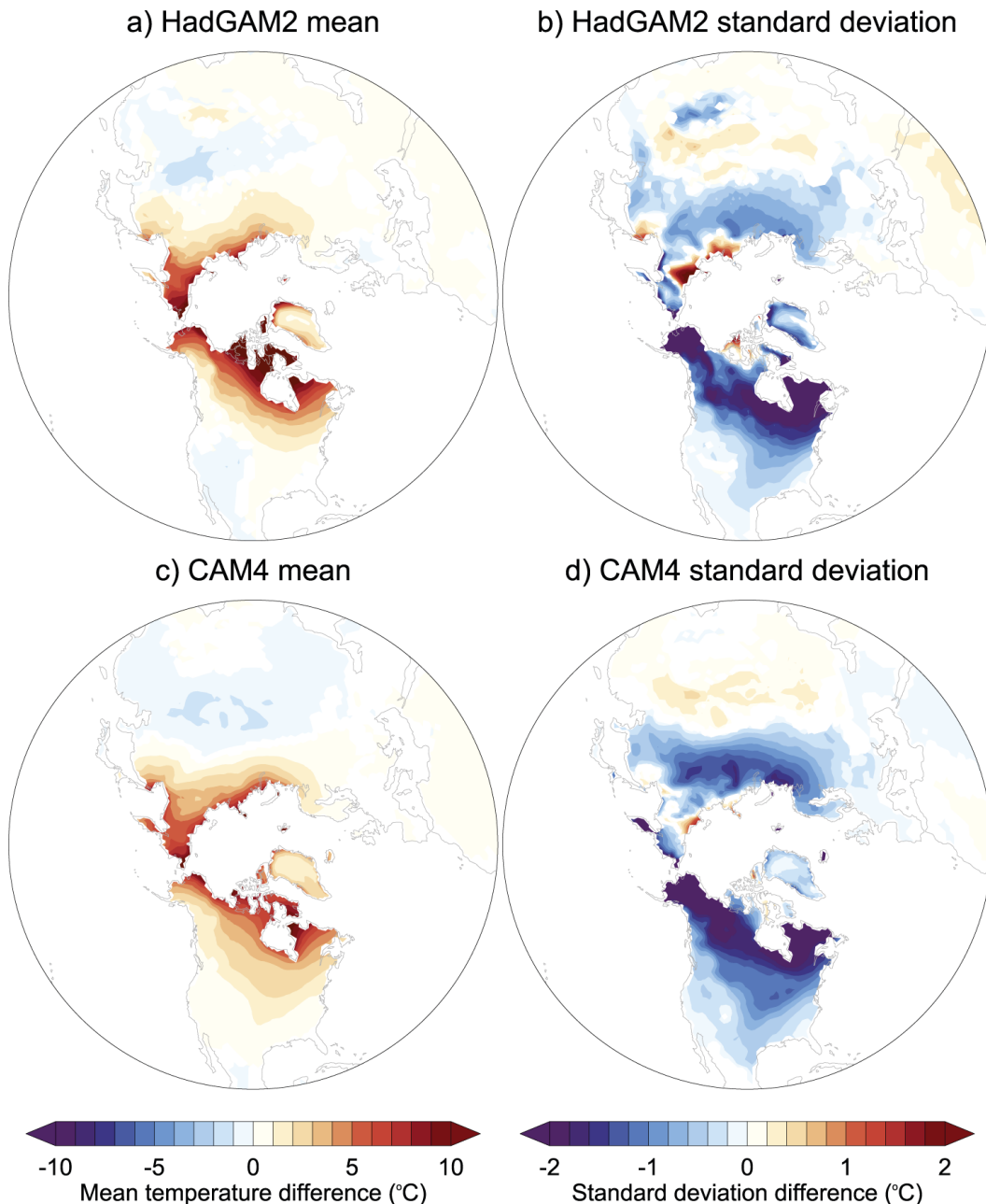Standard deviation difference (°C)

FIG. 6. As in Fig. 5, but for differences between the period 2080–99 and 1980–99. Note the different color scales.

explicitly, Fig. 7 presents the spatial pattern of the sea ice–forced change in the probability of cold extremes. Here, the temperature threshold is calculated as the 1.1 percentile of the late C20 distribution at each grid point. For clarity in Fig. 7, we simplify these probability changes into broad categories that emphasize the sign and relative magnitude of the sea ice–forced change from the late C20. Focusing first on the changes by the mid-C21, both models depict reduced probabilities of cold extremes over the high latitudes (Figs. 7a,c). The midlatitude responses are dissimilar in the two models. For example, HadGAM2 shows reduced probability

over the majority of North America, whereas CAM4 depicts comparably large reductions over northern and eastern North America but modest increases over southern and western parts of the continent. The late C21 changes are in very good agreement between the models, however (Figs. 7b,d). This suggests that the discrepancies in the mid-C21 responses arise due to the small signal-to-noise ratio and not model differences in the forced response. By the late C21 both models simulate large probability reductions over North America, Europe, and Russia. In parts of northern Canada and northeast Asia, the probability reduces to zero, and
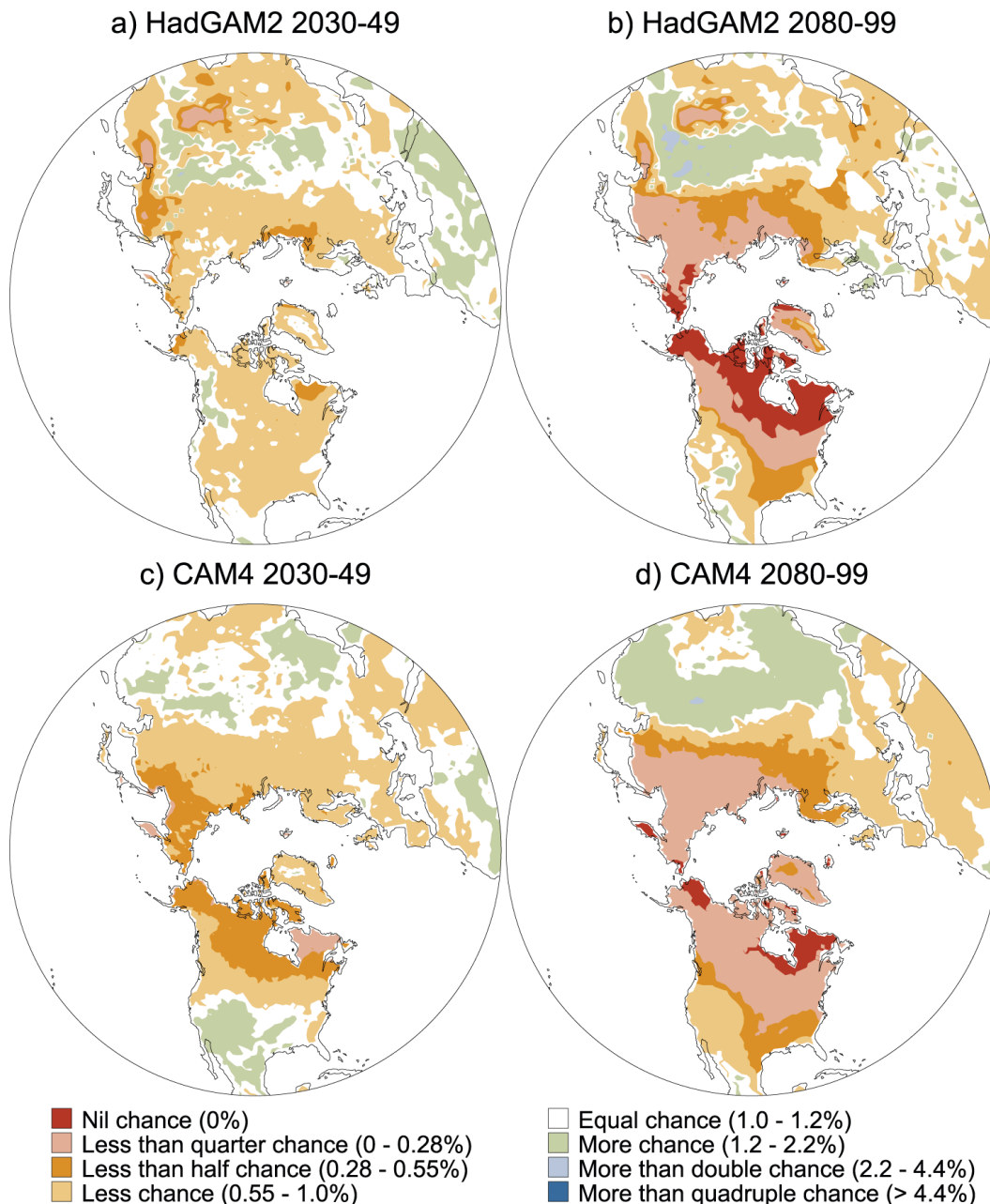
a) HadGAM2 2030-49   b) HadGAM2 2080-99

c) CAM4 2030-49   d) CAM4 2080-99

Legend:
- ◼ Nil chance (0%)
- ◼ Less than quarter chance (0 - 0.28%)
- ◼ Less than half chance (0.28 - 0.55%)
- ◼ Less chance (0.55 - 1.0%)
- ◻ Equal chance (1.0 - 1.2%)
- ◼ More chance (1.2 - 2.2%)
- ◼ More than double chance (2.2 - 4.4%)
- ◼ More than quadruple chance (> 4.4%)

FIG. 7. (a) Probability of extreme cold (winter daily temperature as cold or colder than the 1.1 percentile during the period 1980–99) in the sea ice–forced HadGAM2 simulation for the period 2030–49. Colored shading categories are based on the relative change in probability compared to the period 1980–99. (b) As in (a), but for the period 2080–99 relative to 1980–99. (c),(d) As in (a),(b), but for the sea ice–forced CAM4 simulations.

over large swaths of North America and northern Asia, the probability is more than halved. Both models show slightly increased probabilities over central and southern Asia, although the exact regions differ, related cooling is induced by a strengthened Siberian high.

So far we have only considered the changing probability of extremely cold days. There has been recent speculation that Arctic warming and sea ice loss may increase the frequency of longer-duration cold extremes

as a result of more persistent weather patterns over North America (Francis and Vavrus 2012). Motivated by this, we have also examined the changing probability of 5-day and 9-day cold extremes (Fig. 8). The simulated changes in the frequency of these longer-duration extremes closely match those shown previously for daily extremes (as do the patterns of standard deviation change; not shown). Therefore, our simulations do not support the hypothesis of more frequent cold spells over
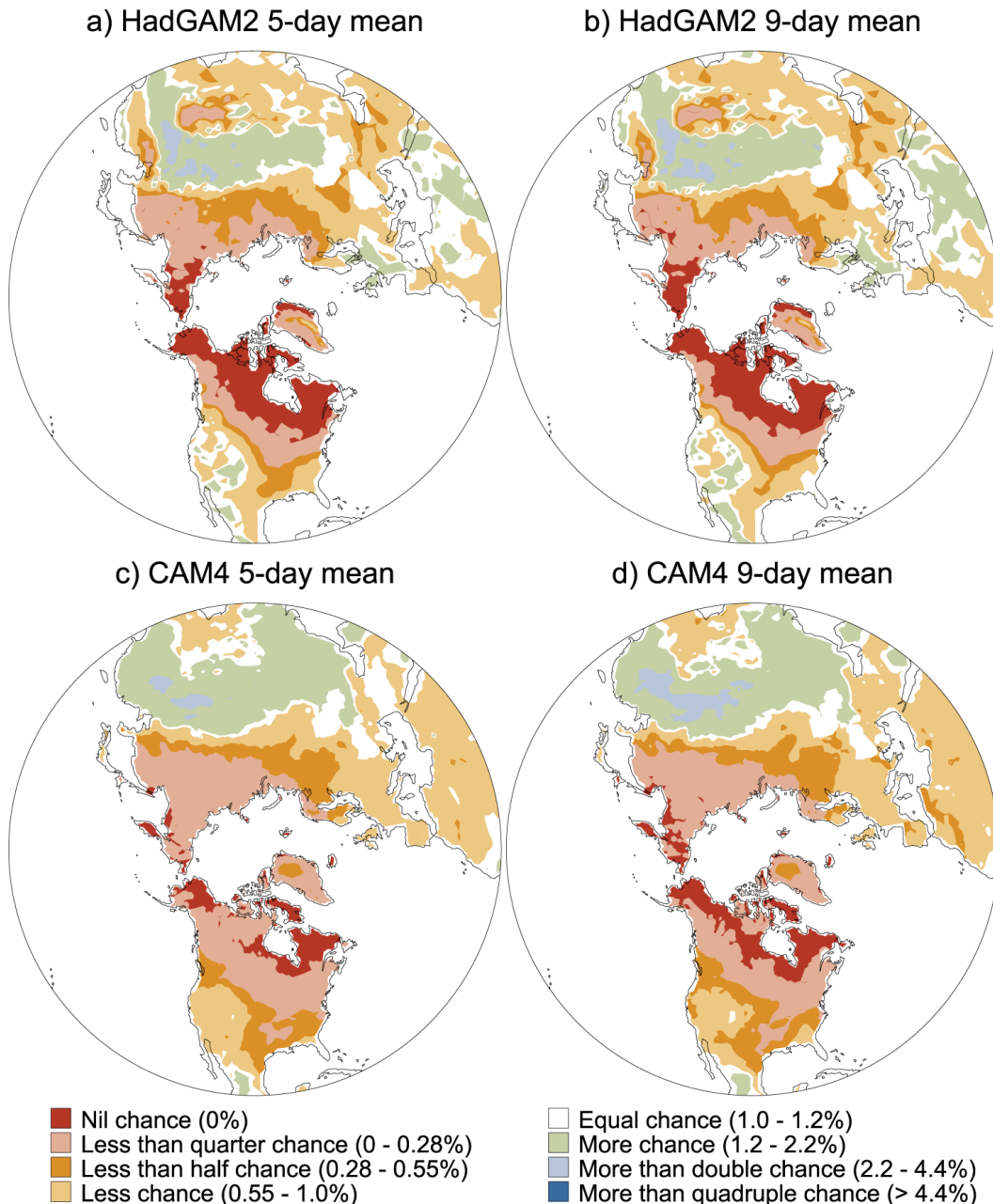
a) HadGAM2 5-day mean   **b) HadGAM2 9-day mean**

c) CAM4 5-day mean   **d) CAM4 9-day mean**

■ Nil chance (0%)	□ Equal chance (1.0 - 1.2%)
■ Less than quarter chance (0 - 0.28%)	■ More chance (1.2 - 2.2%)
■ Less than half chance (0.28 - 0.55%)	■ More than double chance (2.2 - 4.4%)
■ Less chance (0.55 - 1.0%)	■ More than quadruple chance (> 4.4%)

Fɪɢ. 8. (a) Probability of extreme cold (winter 5-day mean temperature as cold or colder than the 1.1 percentile during the period 1980–99) in the sea ice–forced HadGAM2 simulation for the period 2080–99. Colored shading categories are based on the relative change in probability compared to the period 1980–99. (b) As in (a), but for 9-day means. (c),(d) As in (a),(b), but for the sea ice–forced CAM4 simulations.

central and eastern North America in response to sea ice loss. They do suggest that, in isolation, Arctic sea ice loss favors increased cold spells over central Asia, consistent with Mori et al. (2014). However, it should be noted that the net effect of GHG increases is to reduce the chance of central Asian cold extremes (Mori et al. 2014).

CONCLUDING REMARKS. We have used large ensembles of model simulations to explore how the risk

of North American daily cold extremes is anticipated to change in the future in response to increases in GHG and the component of that response solely due to Arctic sea ice loss. Specifically, we have examined the changing probability of daily cold extremes as (un)common as the 7 January 2014 event. Projected increases in GHG will decrease the likelihood of North American cold extremes in the future. Days as cold or colder than 7 January 2014 are still projected to occur in the

mid-C21 (2030–49), albeit less frequently than in the late C20 (1980–99). However, such events will cease to occur by the late C21 (2080–99), assuming GHG emissions continue unabated. Continued Arctic sea ice loss is a major driver of decreased—not increased—North America cold extremes. Projected Arctic sea ice loss alone reduces the odds of such an event by one-quarter to one-third in the mid-C21 compared to late C20 and to zero (or near zero) by the late C21. Both projected mean warming and a decrease in temperature variability contribute to the decrease in daily cold extremes.

Recent claims that Arctic sea ice loss may increase the risk of midlatitude cold extremes are primarily based on hypothesized increases in the latitudinal extent of north–south excursions of the jet stream. The simple reasoning is that a more meandering jet stream will increase the frequency of cold Arctic air migrating southward and thus lead to more frequent cold extremes in the midlatitudes. However, this logic ignores two important factors, even putting aside the considerable uncertainty in future changes in the jet stream (Barnes and Polvani 2013) and associated features of the atmospheric circulation (Masato et al. 2013). The first factor ignored is that the midlatitudes are warming. This means it takes a larger-magnitude cold anomaly to cause a cold extreme than in a cooler climate. The second factor ignored is that disproportionally large warming of the high latitudes compared to the midlatitudes reduces the average temperature gradient between these two regions. This means that if an Arctic air mass is displaced southward into the midlatitudes, then the resulting temperature anomaly is smaller than is the case for a larger north–south temperature gradient. These two factors translate into a reduced chance of cold extremes. Our results suggest these thermodynamically induced changes are of first-order importance in determining the future risk of cold extremes and that dynamically induced changes play a secondary role (such as changes in the behavior of the jet stream). As a result, we should expect fewer—and not more—cold extremes over the coming decades in the midlatitudes including North America.

REFERENCES

Alexander, L. V., and Coauthors, 2006: Global observed changes in daily climate extremes of temperature and precipitation. *J. Geophys. Res.,* **111,** D05109, doi:10.1029/2005JD006290.

Barnes, E. A., 2013: Revisiting the evidence linking Arctic amplification to extreme weather in midlatitudes. *Geophys. Res. Lett.,* **40,** 4728–4733, doi:10.1002/grl.50880.

——, and L. M. Polvani, 2013: Response of the midlatitude jets, and of their variability, to increased greenhouse gases in the CMIP5 models. *J. Climate,* **26,** 7117–7135, doi:10.1175/JCLI-D-12-00536.1.

——, E. Dunn-Sigouin, G. Masato, and T. Woollings, 2014: Exploring recent trends in Northern Hemisphere blocking. *Geophys. Res. Lett.,* **41,** 638–644, doi:10.1002/2013GL058745.

Cohen, J., and Coauthors, 2014: Recent Arctic amplification and extreme mid-latitude weather. *Nat. Geosc.,* **7,** 627–637, doi:10.1038/ngeo2234.

Collins, W. J., and Coauthors, 2011: Development and evaluation of an Earth-System model—HadGEM2. *Geophys. Model Dev.,* **4,** 1051–1075, doi:10.5194/gmd-4-1051-2011.

Deser, C., R. Tomas, M. Alexander, and D. Lawrence, 2010: The seasonal atmospheric response to projected Arctic sea ice loss in the late twenty-first century. *J. Climate,* **23,** 333–351, doi:10.1175/2009JCLI3053.1.

——, ——, and L. Sun, 2015: The role of ocean–atmosphere coupling in the zonal-mean atmospheric response to Arctic sea ice loss. *J. Climate,* **28,** 2168–2186, doi:10.1175/JCLI-D-14-00325.1.

Donat, M. G., and Coauthors, 2013: Updated analyses of temperature and precipitation extreme indices since the beginning of the twentieth century: The HadEX2 dataset. *J. Geophys. Res. Atmos.,* **118,** 2098–2118, doi:10.1002/jgrd.50150.

Fischer, E. M., and R. Knutti, 2014: Heated debate on cold weather. *Nat. Climate Change,* **4,** 537–538, doi:10.1038/nclimate2286.

Francis, J. A., and S. J. Vavrus, 2012: Evidence linking Arctic amplification to extreme weather in mid-latitudes. *Geophys. Res. Lett.,* **39,** L06801, doi:10.1029/2012GL051000.

Gent, P. R., and Coauthors, 2011: The Community Climate System Model version 4. *J. Climate,* **24,** 4973–4991, doi:10.1175/2011JCLI4083.1.

Gerber, F., J. Sedláček, and R. Knutti, 2014: Influence of the western North Atlantic and the Barents Sea on European winter climate. *Geophys. Res. Lett.,* **41,** 561–567, doi:10.1002/2013GL058778.

Hassanzadeh, P., Z. Kuang, and B. F. Farrell, 2014: Responses of midlatitude blocks and wave amplitude

to changes in the meridional temperature gradient in an idealized dry GCM. *Geophys. Res. Lett.,* **41,** 5223–5232, doi:10.1002/2014GL060764.

Honda, M., J. Inoue, and S. Yamane, 2009: Influence of low Arctic sea-ice minima on anomalously cold Eurasian winters. *Geophys. Res. Lett.,* **36,** L08707, doi:10.1029/2008GL037079.

Inoue, J., M. E. Hori, and K. Takaya, 2012: The role of Barents Sea ice in the wintertime cyclone track and emergence of a warm-Arctic cold-Siberian anomaly. *J. Climate,* **25,** 2561–2568, doi:10.1175/JCLI-D-11-00449.1.

Kalnay, E., and Coauthors, 1996: The NCEP/NCAR 40-Year Reanalysis Project. *Bull. Amer. Meteor. Soc.,* **77,** 437–471, doi:10.1175/1520-0477(1996)077<0437:TNYRP>2.0.CO;2.

Kharin, V. V., F. W. Zwiers, X. Zhang, and G. C. Hegerl, 2007: Change in daily temperature and precipitation extremes in the IPCC ensemble of global coupled model simulations. *J. Climate,* **20,** 1419–1444, doi:10.1175/JCLI4066.1.

——, ——, ——, and M. Wehner, 2013: Changes in temperature and precipitation extremes in the CMIP5 ensemble. *Climatic Change,* **119,** 345–357, doi:10.1007/s10584-013-0705-8.

Liu, J., J. A. Curry, H. Wang, M. Song, and R. M. Horton, 2012: Impact of declining Arctic sea ice on winter snowfall. *Proc. Natl. Acad. Sci. USA,* **109,** 4074–4079, doi:10.1073/pnas.1114910109.

Masato, G., B. J. Hoskins, and T. Woollings, 2013: Winter and summer Northern Hemisphere blocking in CMIP5 models *J. Climate,* **26,** 7044–7059, doi:10.1175/JCLI-D-12-00466.1.

Mori, M., M. Watanabe, H. Shiogama, J. Inoue, and M. Kimoto, 2014: Robust Arctic sea-ice influence on the frequent Eurasian cold winters in past decades. *Nat. Geosci.,* **7,** 869–873, doi:10.1038/ngeo2277.

Peings, Y., and G. Magnusdottir, 2014: Response of the wintertime Northern Hemisphere atmospheric circulation to current and projected Arctic sea ice decline: A numerical study with CAM5. *J. Climate,* **27,** 244–264, doi:10.1175/JCLI-D-13-00272.1.

Petoukhov, V., and V. A. Semenov, 2010: A link between reduced Barents-Kara sea ice and cold winter extremes over northern continents. *J. Geophys. Res.,* **115,** D21111, doi:10.1029/2009JD013568.

Screen, J. A., 2014: Arctic amplification decreases temperature variance in northern mid- to high-latitudes. *Nat. Climate Change,* **4,** 577–582, doi:10.1038/nclimate2268.

——, and I. Simmonds, 2010a: Increasing fall-winter energy loss from the Arctic Ocean and its role in Arctic temperature amplification. *Geophys. Res. Lett.,* **37,** L16707, doi:10.1029/2010GL044136.

——, and ——, 2010b: The central role of diminishing sea ice in recent Arctic temperature amplification. *Nature,* **464,** 1334–1337, doi:10.1038/nature09051.

——, and ——, 2013: Exploring links between Arctic amplification and mid-latitude weather. *Geophys. Res. Lett.,* **40,** 959–964, doi:10.1002/grl.50174.

——, ——, C. Deser, and R. Tomas, 2013: The atmospheric response to three decades of observed Arctic sea ice loss. *J. Climate,* **26,** 1230–1248, doi:10.1175/JCLI-D-12-00063.1.

——, ——, I. Simmonds, and R. Tomas, 2014: Atmospheric impacts of Arctic sea-ice loss, 1979–2009: Separating forced change from atmospheric internal variability. *Climate Dyn.,* **43,** 333–344, doi:10.1007/s00382-013-1830-9.

Stroeve, J. C., V. Kattsov, A. Barrett, M. Serreze, T. Pavlova, M. Holland, and W. N. Meier, 2012: Trends in Arctic sea ice extent from CMIP5, CMIP3 and observations. *Geophys. Res. Lett.,* **39,** L16502, doi:10.1029/2012GL052676.

Tang, Q., X. Zhang, X. Yang, and J. A. Francis, 2013: Cold winter extremes in northern continents linked to Arctic sea ice loss. *Environ. Res. Lett.,* **8,** 014036, doi:10.1088/1748-9326/8/1/014036.

Taylor, K. E., R. J. Stouffer, and G. A. Meehl, 2012: Overview of CMIP5 and the experiment design. *Bull. Amer. Meteor. Soc.,* **93,** 485–498, doi:10.1175/BAMS-D-11-00094.1.

Vihma, T., 2014: Effects of Arctic sea ice decline on weather and climate: A review. *Surv. Geophys.,* **35,** 1175–1214, doi:10.1007/s10712-014-9284-0.

Wallace, J. M., I. M. Held, D. W. Thompson, K. E. Trenberth, and J. Walsh, 2014: Global warming and winter weather. *Science,* **343,** 729–730, doi:10.1126/science.343.6172.729.

Walsh, J., 2014: Intensified warming of the Arctic: Causes and impacts on middle latitudes. *Global Planet. Change,* **117,** 52–63, doi:10.1016/j.gloplacha.2014.03.003.

Woollings, T., B. Harvey, and G. Masato, 2014: Arctic warming, atmospheric blocking and cold European winter in CMIP5 models. *Environ. Res. Lett.,* **9,** 014002, doi:10.1088/1748-9326/9/1/014002.

Yang, S., and J. H. Christensen, 2012: Arctic sea ice reduction and European cold winters in CMIP5 climate change experiments. *Geophys. Res. Lett.,* **39,** L20707, doi:10.1029/2012GL053338.

Science at Your Fingertips

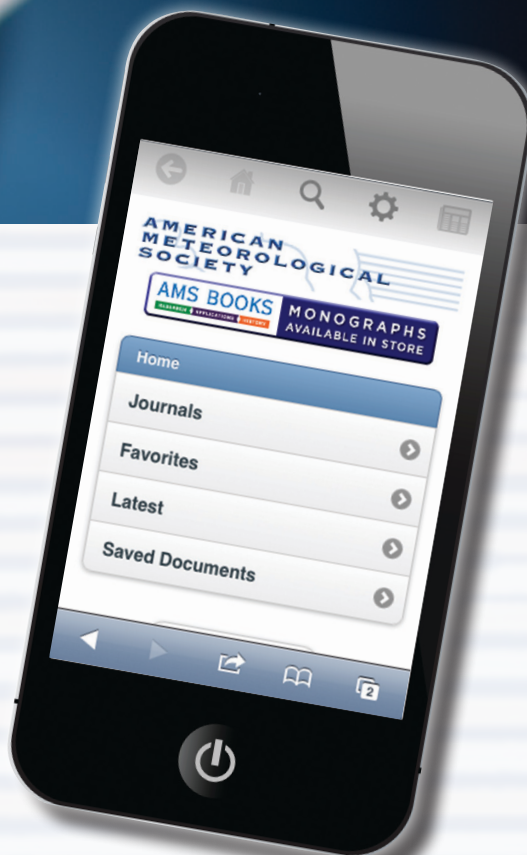**AMS Journals are now optimized for viewing on your mobile device.**
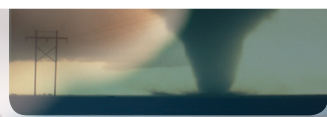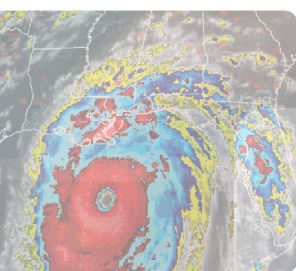
Access journal articles, monograph titles, and BAMS content using your iOS, Android, or Blackberry phone, or tablet.

Features include:

- Saving articles for offline reading
- Sharing of article links via email and social networks
- Searching across journals, authors, and keywords

And much more...

Scan code to connect to
journals.ametsoc.org

AMERICAN METEOROLOGICAL SOCIETY